

Localization of the Site of Origin of Cardiac Activation by Means of a Heart-Model-Based Electrocardiographic Imaging Approach

Guanglin Li and Bin He*, *Senior Member, IEEE*

Abstract—We have developed a new approach to solve the inverse problem of electrocardiography in terms of heart model parameters. The inverse solution of the electrocardiogram (ECG) inverse problem is defined, in the present study, as the parameters of the heart model, which are closely related to the physiological and pathophysiological status of the heart, and is estimated by using an optimization system of heart model parameters, instead of solving the matrix equation relating the body surface ECGs and equivalent cardiac sources. An artificial neural network based preliminary diagnosis system has been developed to limit the searching space of the optimization algorithm and to initialize the model parameters in the computer heart model. The optimal heart model parameters were obtained by minimizing the objective functions, as functions of the observed and model-generated body surface ECGs. We have tested the feasibility of the newly developed technique in localizing the site of origin of cardiac activation using a pace mapping protocol. The present computer simulation results show that, the present approach for localization of the site of origin of ventricular activation achieved an averaged localization error of about 3 mm [for 5- μ V Gaussian white noise (GWN)] and 4 mm (for 10- μ V GWN), with standard deviation of the localization errors of being about 1.5 mm. The present simulation study suggests that this newly developed approach provides a robust inverse solution, circumventing the difficulties of the ECG inverse problem, and may become an important alternative to other ECG inverse solutions.

Index Terms—Body surface potential maps, electrocardiographic imaging, electrocardiography, heart model, inverse problem, optimization algorithms, pace mapping.

I. INTRODUCTION

THE GOAL of the inverse problem of electrocardiography is to noninvasively and quantitatively characterize and reconstruct cardiac electrical events from body surface electrocardiographic measurements. In contrast to the forward problem of electrocardiography, which can be solved uniquely within a constraint, the electrocardiogram (ECG) inverse problem does not possess a mathematically unique solution. Several approaches have been explored to tackle this

challenging problem. Efforts have been made to circumvent the nonuniqueness of the ECG inverse problem by using equivalent cardiac generators (such as equivalent dipoles [1]–[4] and multipoles [5]), heart surface isochrone [6], [7], or epicardial potentials [8]–[17]. Among the ECG inverse solutions, the epicardial inverse solutions have been demonstrated by many investigators to provide important unrestricted information regarding the underlying cardiac electrical activity.

Another characteristic of the ECG inverse problem, not so easily bypassed, is its ill-posed nature whereby the desired inverse solution is unstable and can oscillate wildly with the slightest noise or other perturbation in the electrical and/or geometrical input data. The techniques of regularization must therefore be used to suppress the effects of inevitable errors due to imposing constraints on the solutions. In order to obtain accurate, stable and reliable ECG inverse solutions, investigators have explored techniques of regularization [9]–[14]. Recently, several investigators [15]–[17] have also attempted to solve the ECG inverse problems by employing body surface Laplacian ECG measurements [18], [19].

Although one can circumvent the difficulty that arises from the lack of a mathematically unique solution in the ECG inverse problem and minimize the effects of the inevitable errors by imposing constraints on the solution by means of regularization, some difficulties still exist. For example, it is obvious that even if the ECG inverse solutions, using either the equivalent cardiac-source representation or the epicardial potentials, can be accurately obtained, they are not the desired results which allow us to gauge the physiological or pathophysiological status in the three dimensional myocardium and to establish a clinical diagnosis. One still must deduce or evaluate the cardiac physiological or pathological characteristics inside the three-dimensional (3-D) myocardium from the inverse solutions of either equivalent cardiac generators or heart surface inverse solutions. These difficulties limit the potentially beneficial ECG inverse solutions from becoming a routine clinical tool at present.

In the present investigation, we have developed a new electrocardiographic imaging technique to solve the ECG inverse problem, in terms of the heart-model parameters. We have demonstrated, in the present simulation study, that our new technique can directly obtain the cardiac physiological and pathological characteristics corresponding to the measured body surface ECGs. Our computer simulation results demonstrate the feasibility of our new approach to localize the site of origin of cardiac activation. Such applications may have important clinical applications in locating the site of origin of

Manuscript received June 29, 2000; revised February 26, 2001. This work was supported in part by the National Science Foundation (NSF) under CAREER Award BES-9875344, in part by the American Heart Association under Grant 0140132N, and in part by a grant from the Campus Research Board of the University of Illinois at Chicago. *Asterisk indicates corresponding author.*

G. Li is with the University of Illinois at Chicago, Department of EECS, Chicago, IL 60607 USA.

*B. He is with the University of Illinois at Chicago, Departments of EECS and Bioengineering, SEO 1120, M/C-154, 851 S. Morgan Street, Chicago, IL 60607 USA (e-mail: bhe@uic.edu).

Publisher Item Identifier S 0018-9294(01)04173-8.

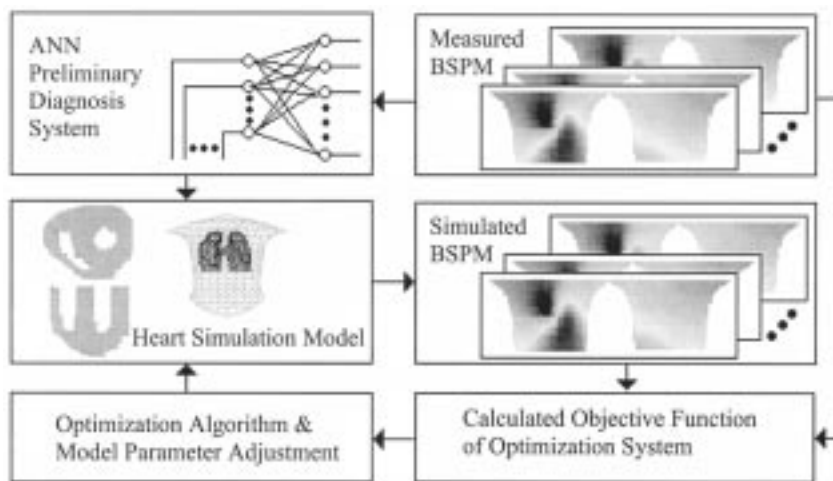


Fig. 1. The schematic diagram of the present heart-model-based electrocardiographic imaging approach for solving the ECG inverse problem in terms of the heart model parameters.

cardiac arrhythmia, for example, the site of accessory pathway (AP) of Wolff–Parkinson–White syndrome (WPW), ventricular tachycardia, and ectopic cardiac beats.

II. METHODS

A. A New Approach for ECG Inverse Problem

The present approach indirectly obtains the ECG inverse solution in terms of heart model parameters using a parameter optimization system. In contrast, other methods directly solve the matrix equation linking the electrical sources with electrical potential fields to estimate the ECG inverse solution. The schematic diagram of the new approach is shown in Fig. 1. A preliminary diagnosis system (PDS) to determine cardiac status based on *a priori* knowledge and the measured BSPM was developed using an artificial neural network (ANN), and is used to obtain initial information on the site of origin of cardiac activation. The output of the ANN-based PDS provides the initial heart model parameters used in the optimization system. Then the body surface potential maps (BSPMs) were simulated using the 3-D computer heart model, and then the objective functions that assess the similarity between the measured and simulated BSPMs were calculated. If the measured BSPM and the simulated BSPM matches well, the heart model parameters corresponding with the simulated BSPM are regarded as the inverse solution of the measured BSPM, from which the site of origin of activation can be uniquely and accurately determined. If not, the heart model parameters are adjusted with the aid of the optimization algorithms and the simulation procedure proceeds until the objective functions satisfy the given convergent criteria. The inverse solutions so obtained are the heart model parameters that directly correspond to the physiological and pathological status in the heart (e.g., the site of origin of cardiac activation, or the site of AP for WPW syndrome).

B. Computer Heart Model and Pacing Protocol

A previously developed computer heart simulation model [20] was used. The geometry model of the heart and torso was

constructed using CT images of a human subject as shown in Fig. 2(a). The torso surface, lung surface, endocardial surface and epicardial surface were divided into 412, 297, 154, and 158 nodes, and 820, 586, 296, and 308 triangles connecting these nodes, respectively. The heart model contains about 65 000 myocardial cell units with a spatial resolution of 1.5 mm as shown in Fig. 2(b). The spatial location of each unit was denoted by a set of three integers (i , j , and k). From the base to the apex, the ventricles are divided into 53 myocardial segments (numbered from $MS-1$ to $MS-53$). Every segment is comprised of approximately the same number of myocardial cell units. The ventricles consist of 50 layers [from Layer 30 to Layer 79 (the whole heart has 80 layers)], with interlayer distance of being 1.5 mm. Layer 30 corresponds to the base and Layer 79 the apex. Each myocardial segment corresponds to a 3-D ventricular myocardial block that includes seven-layers myocardium cell units. For example, in the region adjacent to the atrial-ventricular (AV) ring, there are ten myocardial segments (numbered from $MS-1$ to $MS-10$), which correspond to ventricular myocardium between Layer 30 and Layer 36. The left-top part of Fig. 4 illustrates these ten myocardial segments in one layer, with different gray levels illustrating different myocardial segments.

Twenty-four sites throughout the ventricles were selected to test the performance of the present technique. The BSPMs induced by pacing each of these 24 sites were simulated by means of the boundary element method [21]. For pacing at each of the 24 sites, 200-lead BSPMs [shown in Fig. 2(a)] on the torso surface were calculated at every 3 ms over the ventricular excitation cycle. Fig. 2(c) shows an example of the ventricular excitation sequence after pacing in the anterior wall of the left ventricle.

C. Preliminary Diagnosis System

Application of *a priori* knowledge to limit the searching space of heart model parameters is of vital importance. To achieve this, we developed a *Preliminary Diagnosis System* of cardiac status with *a priori* ECG knowledge. The PDS is developed to approximately determine the cardiac status, which is then used to initialize the heart model parameters and limit the searching

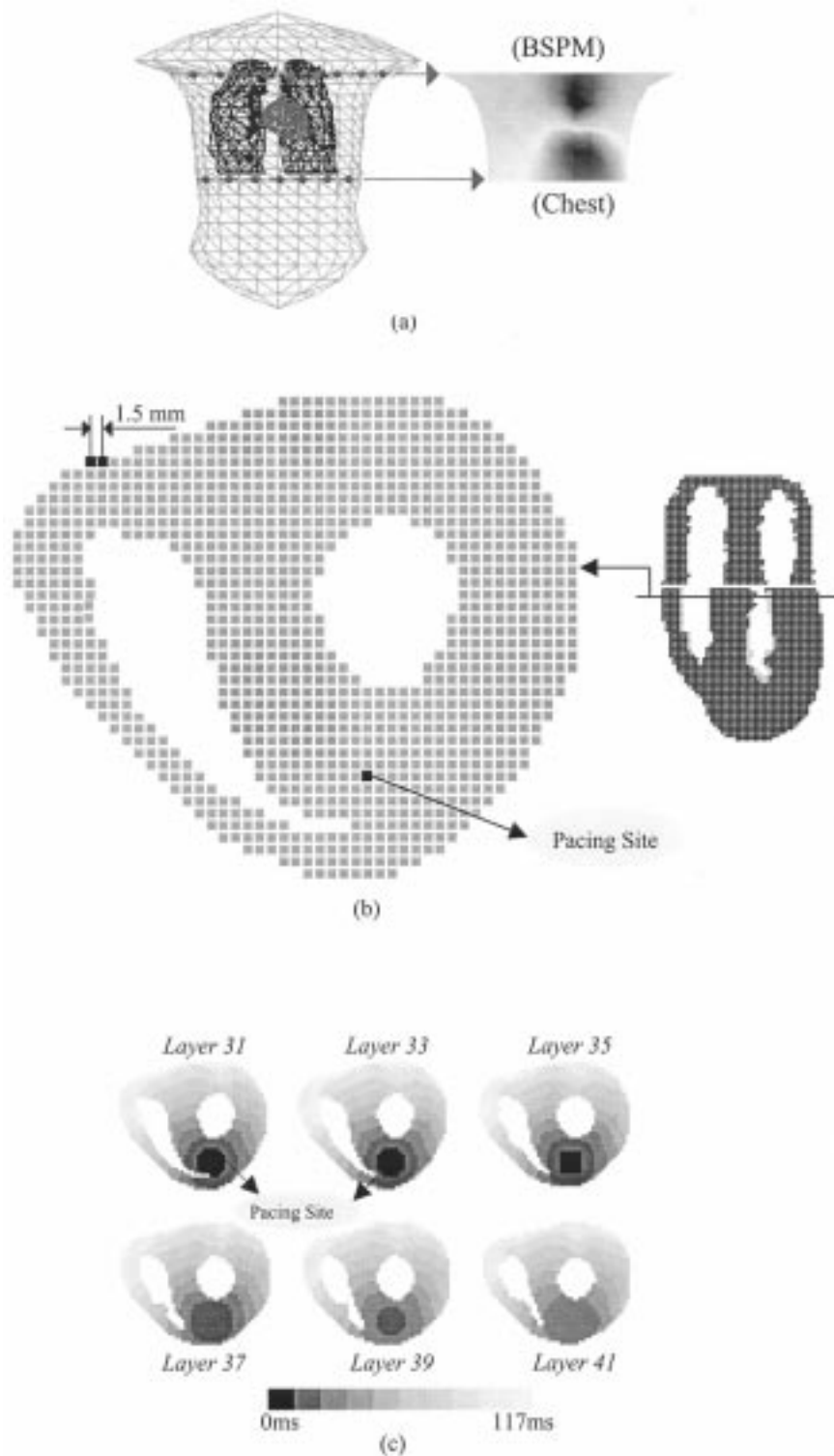


Fig. 2. (a) The computer heart-torso model used in the present simulation study, and an example of the BSPM simulated on the chest at 40 ms following pacing. (b) A horizontal section of the heart model over which the pacing site is illustrated by a black dot. (c) An example of the excitation sequence after pacing on the anterior ventricular wall.

space in the computer heart model for the parameter optimization system.

In the present study, we have developed the PDS based on a three-layer feed-forward ANN as shown in Fig. 3. This ANN is capable of mapping the nonlinear input-output relationship, to a desired degree of accuracy. An adaptively weighted coef-

ficient algorithm [22] was used to train the ANN. The number of neurons in the input layer was set to 200, corresponding to the number of body surface electrodes used in the present simulation study. The hidden layer had 25 neurons that were determined heuristically. The output layer had 53 neurons, which corresponded to 53 ventricular myocardial segments of com-

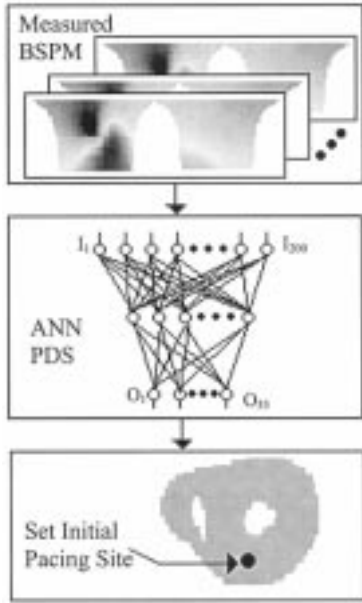


Fig. 3. The block diagram of the preliminary diagnosis system based on a three-layer feed-forward ANN. The input to the PDS is the BSPMs at 200 body surface electrodes over time, and the output from the PDS is the region inside myocardium, which provides the initial pacing site in the parameter optimization. The input, hidden and output layers of the ANN have 200, 25, and 53 neurons, respectively.

puter heart model: *MS-1* to *MS-53*. Five cardiac cellular units were selected for each of 53 myocardial segments in the ventricles, and each of these $5 \times 53 = 265$ sites was then paced in the forward simulation using the computer heart-torso model, generating the dataset for training the ANN. Each of these 265 training sites was different with the 24 testing pacing sites in the present simulation. Noise added BSPMs were used to simulate noise-contaminated body surface ECG measurements. The BSPM maps at five time instants during 25 to 50 ms after initial activation were used as inputs to train the ANN.

D. Objective Functions

We localized the site of origin of cardiac activation by minimizing dissimilarity between the measured and heart-model-generated BSPMs. The dissimilarity between the measured and simulated BSPMs could be described by appropriate characteristic parameters extracted from the BSPMs. The characteristic parameters should be selected in such a way that they are highly sensitive to the different sites of ectopic activation, and insensitive to the intersubject variation. In the present study, the following three objective functions were used to reflect the dissimilarity between the measured and simulated BSPMs for localization of site of ectopic activation.

- 1) $E_{CC}(x)$, which was constructed with the average correlation coefficient (CC) between the measured and simulated BSPMs from instant T_1 to instant T_2 of the cardiac excitation after detection of initial activation, is defined as

$$E_{CC}(x) = \sum_{t=T_1}^{T_2} [1 - CC_{ms}(x, t)] / (T_2 - T_1) \quad (1)$$

where $CC_{ms}(x, t)$ is the CC between the measured and simulated BSPMs at instant t . x is a parameter vector of the spatial location of initial activation in the computer heart model.

- 2) $E_{\min p}(x)$, which was constructed with the deviation of the positions of minima of the measured and simulated BSPMs from instant T_1 to instant T_2 , is defined as

$$E_{\min p}(x) = \sum_{t=T_1}^{T_2} \|P_{\min}^M(t) - P_{\min}^S(x, t)\| \quad (2)$$

where $P_{\min}^M(t)$ and $P_{\min}^S(x, t)$ represent the positions of the minima in the measured and simulated BSPMs at instant t , respectively. The definition of x is the same as that in (1).

- 3) $E_{NPL}(x)$, which was constructed with the relative error of the number of body surface recording leads, at which the potentials are less than a certain negative threshold, in the measured and simulated BSPMs from instant T_1 to instant T_2 , is defined as

$$E_{NPL}(x) = \left(\sum_{t=T_1}^{T_2} L_N^M(t) - \sum_{t=T_1}^{T_2} L_N^S(x, t) \right) / \sum_{t=T_1}^{T_2} L_N^M(t) \quad (3)$$

where $L_N^M(t) = \sum_{i=1}^{N_L} u(\phi_T - \phi(t, i))$ and $L_N^S(x, t) = \sum_{i=1}^{N_L} u(\phi_T - \phi(x, t, i))$, are the numbers of recording leads, at which the potentials are less than a given threshold $\phi_T (< 0)$, in the measured and simulated BSPMs at instant t , respectively; $\phi(t, i)$ and $\phi(x, t, i)$ are the i th-lead measured and simulated potentials at instant t , respectively; $u(\bullet)$ is the unit-step function, which gives a unity output if the potential at a lead is less than the preset threshold; and N_L is the number of body surface recording leads. The definition of x is the same as that in (1).

The present selection of three objective functions relied heavily on the morphologies, location of the minimum, and the area of negativity in the BSPMs. This is because the BSPM pattern and the site of negativity change with the site of initial activity and not so much the site of positivity. Also, it has been reported [23], [24] that little influence to the morphology and site of negativity was observed due to individual difference. Note that the present objective functions were particularly selected for the localization of site of ectopic activation, and will need be changed for a different cardiac pathology, since the optimal characteristic parameters will be different for different cardiac pathologies.

E. Optimization Algorithm

Optimization of the heart model parameters is a multiobjective nonlinear optimizing problem. Let the objective function of the entire optimization system be $E(x) = f(E_{CC}(x), E_{\min p}(x), E_{NPL}(x))$, the mathematical

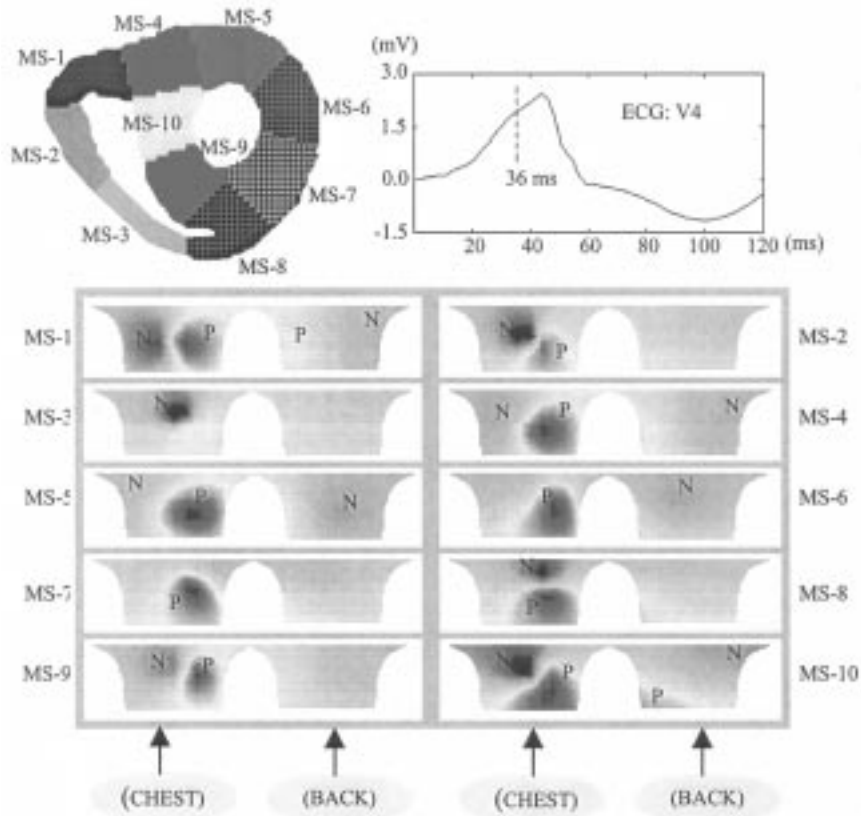


Fig. 4. An example of the simulated BSPMs induced by pacing at ten myocardial segments (*MS-1* to *MS-10*) in the ventricular base along AV-ring, at 36 ms following pacing. A representative paced ECG (lead V4 in the 12-lead ECG) obtained by pacing at a site of *MS-2* is shown at the right top. The time instant of 36 ms after pacing is indicated by a vertical dashed line. Note the difference in the morphology of the BSPMs corresponding to the different pacing sites. *P*: positive activity; *N*: negative activity.

model of the desired optimization can then be represented as the following minimization problem

$$\begin{aligned} & \min_{x \in X} (E(x)) \\ & = \min_{x \in X} f(E_{CC}(x), E_{\min p}(x), E_{NPL}(x)) \quad (4) \end{aligned}$$

where X is the probable value region of the parameters in the heart model. x is a parameter vector of the sites of origin of activation in the heart model. We solved this minimization problem by transferring two objective functions into the constraints. Regarding $E_{\min p}(x)$ and $E_{NPL}(x)$ as the constraints, the three-objective nonlinear optimization problem (4) is then converted into the following single-objective nonlinear optimization problem with two constraints

$$\begin{aligned} & \min_{x \in X} (E_{CC}(x)) \\ & = E_{CC}^*, E_{\min p}(x) < \varepsilon_{\min p}, E_{NPL}(x) < \varepsilon_{NPL} \quad (5) \end{aligned}$$

where E_{CC}^* is the optimal value of the objective function $E_{CC}(x)$. $\varepsilon_{\min p}$ and ε_{NPL} are the allowable errors of the objective function $E_{\min p}(x)$ and $E_{NPL}(x)$, respectively. The selection of the $\varepsilon_{\min p}$ or ε_{NPL} will affect the recognition accuracy and convergence rate of the optimization system. The smaller the $\varepsilon_{\min p}$ or ε_{NPL} , the higher the recognition accuracy

and the slower the convergence. On the other hand, because the measured BSPMs will inevitably be contaminated by noise and the accuracy of the simulated BSPMs will also inevitably be limited by the accuracy of a heart-simulation-model, it is possible that the optimization system can not converge or converge to an incorrect site for an excessively small $\varepsilon_{\min p}$ or ε_{NPL} . Note that the $\varepsilon_{\min p}$ and ε_{NPL} are not very sensitive parameters to the present technique since they are only constraint conditions in (5). In the present study, the Simplex Method [25] was used to solve (5).

III. RESULTS

A. Initial Pacing Sites Determined by PDS

The BSPMs induced by pacing at each of the ventricular myocardial segments were simulated using the computer heart model. An example of the BSPMs associated with ten myocardial segments (*MS-1* to *MS-10*) in the ventricular base at 36 ms following pacing at each of the MS is shown in Fig. 4. It is noted that the BSPM spatial patterns show morphological differences corresponding to each MS where the myocardial activation originates. Fig. 4 agrees with experimental observation of Benson *et al.* [23] and Dubuc *et al.* [24] in which the BSPM results were clinically measured in WPW patients, and the simulation results of Hren *et al.* [26]. From these differences in the spatial pattern in the BSPMs, the PDS estimated the myocardial segment where the ventricular activation originates.

TABLE I
COMPUTER SIMULATION RESULTS OF THE PERFORMANCE OF PDS

True Pacing Site (i, j, k)	True MS (No.)	Estimated MS (No.)	True Pacing Site (i, j, k)	True MS (No.)	Estimated MS (No.)
(30, 33, 31)	MS-8	MS-8	(38, 18, 6)	MS-12	MS-12
(30, 31, 13)	MS-3	MS-3	(38, 8, 28)	MS-15	MS-15
(30, 10, 10)	MS-1	MS-1	(40, 30, 34)	MS-18	MS-18
(31, 8, 31)	MS-5	MS-5	(41, 5, 32)	MS-15	MS-15
(31, 38, 24)	MS-8	MS-8	(41, 25, 45)	MS-17	MS-17
(32, 10, 38)	MS-6	MS-6	(43, 13, 8)	MS-11	MS-11
(33, 14, 23)	MS-10	MS-10	(45, 20, 18)	MS-30	MS-20
(34, 24, 8)	MS-2	MS-2	(50, 29, 28)	MS-28	MS-28
(34, 34, 38)	MS-8	MS-8	(50, 8, 25)	MS-24	MS-24
(35, 13, 46)	MS-6	MS-6	(55, 19, 25)	MS-40	MS-40
(36, 32, 35)	MS-8	MS-8	(59, 16, 42)	MS-44	MS-30
(37, 21, 19)	MS-20	MS-20	(60, 23, 32)	MS-47	MS-47

TABLE II
SIMULATION RESULTS OF LOCALIZATION OF THE SITE OF ORIGIN OF VENTRICULAR ACTIVATION

Ventricular Region	True Pacing Site (i, j, k)	Initial Estimate (i, j, k)	Inverse Solution (i, j, k)	Spatial Distance	Iteration Number
BA	(30, 33, 31)	(33, 34, 31)	(31, 32, 31)	2.12 mm	5
BRW	(30, 31, 13)	(33, 33, 16)	(30, 32, 13)	1.50 mm	8
BP	(30, 10, 10)	(33, 9, 8)	(30, 9, 8)	3.35 mm	4
BP	(31, 8, 31)	(33, 5, 34)	(32, 8, 32)	2.12 mm	7
BA	(31, 38, 24)	(33, 34, 31)	(33, 36, 25)	4.50 mm	9
BLW	(32, 10, 38)	(33, 13, 43)	(33, 11, 38)	2.12 mm	8
BS	(33, 14, 23)	(33, 16, 21)	(33, 14, 22)	1.50 mm	4
BRW	(34, 24, 8)	(33, 21, 6)	(33, 24, 7)	2.12 mm	5
BA	(34, 34, 38)	(33, 34, 31)	(33, 34, 37)	2.12 mm	5
BLW	(35, 13, 46)	(33, 13, 43)	(37, 13, 45)	3.35 mm	6
BA	(36, 32, 35)	(33, 34, 31)	(34, 34, 35)	4.24 mm	6
BS	(37, 21, 19)	(40, 17, 21)	(36, 22, 18)	2.60 mm	16
BRW	(38, 18, 6)	(40, 22, 7)	(40, 21, 7)	5.61 mm	3
BP	(38, 8, 28)	(40, 6, 34)	(36, 7, 28)	3.35 mm	14
MA	(40, 30, 34)	(40, 34, 31)	(38, 33, 36)	6.18 mm	12
MP	(41, 5, 32)	(40, 6, 34)	(41, 6, 33)	2.12 mm	4
MLW	(41, 25, 45)	(40, 26, 41)	(41, 26, 43)	3.35 mm	3
MP	(43, 13, 8)	(40, 10, 9)	(43, 13, 9)	1.50 mm	7
MS	(45, 20, 18)	(40, 17, 21)	(45, 18, 20)	4.24 mm	7
AA	(50, 29, 28)	(47, 33, 31)	(49, 30, 28)	2.12 mm	8
AP	(50, 8, 25)	(47, 9, 20)	(51, 9, 25)	2.12 mm	6
AS	(55, 19, 25)	(54, 19, 24)	(54, 19, 24)	2.12 mm	4
ALW	(59, 16, 42)	(47, 17, 21)	(56, 16, 42)	4.50 mm	4
AA	(60, 23, 32)	(61, 19, 27)	(60, 23, 29)	4.50 mm	10

After training the ANN using the sample set of the BSPMs, the 24 cellular units in the ventricles were randomly chosen as the pacing sites. Gaussian white noise (GWN) of 5- μ V or 10- μ V noise level was added to the calculated BSPMs to simulate noise-contaminated BSPMs, which serve as the input data of the PDS. The output of the PDS is the location of the possible site of pacing, in terms of the number of the myocardial segment (from one to 53 in the present study). Table I shows the performance of the PDS when 5- μ V GWN was added to the BSPMs. From Table I, it can be seen that the recognition accuracy of the PDS was around 92%, suggesting its feasibility. In the case that the PDS could not correctly recognize the myocardial segment of pacing site [for example, at the pacing site (45, 20, 18) (MS-30)], the PDS estimation was still close to the location of the true MS (e.g., MS-20 in this case).

According to the results of the PDS, an initial pacing site was set at the center point of the PDS-predicted myocardial segment in the optimization procedure. The initial pacing points for all 24 pacing sites are shown in Table II.

B. Inverse Results of the Recovered Pacing Sites

In the present simulation study, the following parameters were used for the optimization system: 1) $T_1 = 21$ ms and $T_2 = 48$ ms following pacing. In other words, the BSPMs at ten instants were used to localize the site of origin of cardiac activation. 2) The convergence criteria of the optimization system was set at $E_{CC}^* \leq 0.004$, and the allowable errors of the objective functions $E_{\min P}(x)$ and $E_{NPL}(x)$, which were regarded as the constraints, were $\epsilon_{\min P} \leq 1.5$ mm and $\epsilon_{NPL} \leq 0.05$, respectively. 3) Gaussian white noise, with

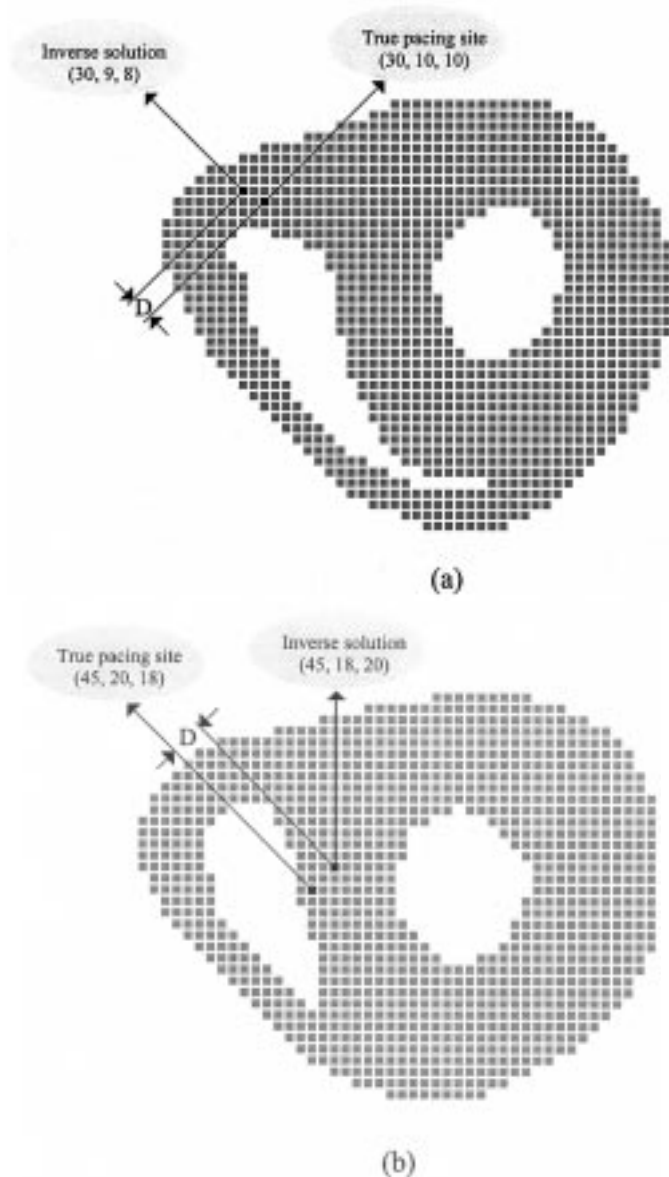


Fig. 5. Two typical examples of the inversely recovered site of origin of activation. (a) The spatial distance between the true and estimated pacing site is 3.35 mm. (b) The spatial distance between the true and estimated pacing site is 4.24 mm.

standard deviation of $5\text{-}\mu\text{V}$ and $10\text{-}\mu\text{V}$, was added to the BSPMs simulated by the computer heart model.

Fig. 5(a) and (b) illustrates two typical examples of the inversely recovered site of origin of ventricular activation. In Fig. 5(a), the known “true” pacing site was in the basal posterior region located at (30, 10, 10) of the right ventricle in the computer heart model, the initial pacing site was set at the center point (33, 9, 8) of *MS-1* according to the result of the PDS, and the site of origin of the ventricular activation, inversely localized by the present optimization algorithm, was in the basal right-posterior region located at (30, 9, 8) in the heart computer model. The spatial distance between the “true” pacing site and the inversely localized site of origin of activation, was 3.35 mm for this case. In Fig. 5(b), the “true” pacing site was in the middle septal region located at

(45, 20, 18) of the ventricle in the computer heart model, the initial pacing site was set at the center point (47, 17, 22) of *MS-8* according to the result of the PDS, and the site of origin of activation, inversely localized by the present optimization algorithm, was in the middle septal region located at (45, 18, 20) in the computer heart model. The spatial distance between the “true” and inverse site of origin of activation was 4.24 mm for this case.

Table II shows the inverse results for all 24 pacing sites when $5\text{-}\mu\text{V}$ GWN was added to the BSPMs. According to the anatomic structure of the ventricles and recommended segmenting methods [27] for the ventricles, the ventricles were divided in the following way. The atrial-ventricular ring was divided into five regions: Anterior, Left Wall, Posterior, Right Wall, and Septum. The ventricle from base to apex was divided into three regions: Basal, Middle, and Apical. For example, BA in Table II means that the pacing site is located in the basal-anterior, and MLW in the middle left wall. From Table II, the mean value and standard deviation of the spatial distance between the true pacing point and the localized site of origin of ventricular activation are 3.04 and 1.32 mm, respectively. The maximum and minimum values of the spatial distance are 6.18 and 1.50 mm, respectively. Table III shows the inverse results for all 24 pacing sites when $10\text{-}\mu\text{V}$ GWN was added to the BSPMs. From Table III, the spatial distance between the true pacing point and the localized site of origin of ventricular activation is 3.88 ± 1.38 mm, and the maximum and minimum values of the spatial distance are 6.18 mm and 2.12 mm, respectively. Tables II and III demonstrate the feasibility of accurately localizing the site of origin of ventricular activation by means of the present heart-model-based electrocardiographic imaging approach.

C. Effects of Heart-Torso Geometry Uncertainties

The effects of the intersubject torso-geometry variation on the performance of the present approach were evaluated by using modified torso models: 10% enlargement and reduction of the normal torso model (NTM+10% and NTM-10%) in the computer heart-torso model. The heart position uncertainty was simulated by moving the heart along horizontal directions of the torso (along the x -direction (from the right to the left) and the y -direction (from the front to the back)). Four new heart positions, the right/left shift along the x -direction (RSX/LSX) and the front/back shift along the y -direction (FSY/BSY), were considered. In all four cases, a distance of 10 mm was shifted.

Five pacing sites, in five different regions adjacent to the AV-ring, were selected from the 24 pacing sites to test the effects of heart-torso geometry uncertainties on the performance of the present approach. The modified torso models were used in the forward BSPM simulation and $10\text{-}\mu\text{V}$ GWN was added into the simulated BSPMs as the measured ECGs. Similarly, for each of four shifted heart positions, the forward simulation was conducted, and $10\text{-}\mu\text{V}$ GWN added into the simulated BSPMs as the measured ECGs. By using the modified heart-torso models in the forward simulations and the standard model in the inverse calculation, the effect of intersubject geometry variation on the present approach was initially evaluated.

TABLE III
SIMULATION RESULTS OF LOCALIZATION OF THE SITE OF ORIGIN OF VENTRICULAR ACTIVATION

Ventricular Region	True Pacing Site (<i>i, j, k</i>)	Initial Estimate (<i>i, j, k</i>)	Inverse Solution (<i>i, j, k</i>)	Spatial Distance	Iteration Number
BA	(30, 33, 31)	(33, 34, 31)	(33, 31, 31)	5.41 mm	4
BRW	(30, 31, 13)	(33, 33, 16)	(30, 33, 13)	3.00 mm	7
BP	(30, 10, 10)	(33, 9, 8)	(31, 9, 8)	3.67 mm	3
BP	(31, 8, 31)	(33, 5, 34)	(33, 9, 33)	4.50 mm	6
BA	(31, 38, 24)	(33, 34, 31)	(33, 35, 26)	6.18 mm	7
BLW	(32, 10, 38)	(33, 13, 43)	(33, 11, 39)	2.59 mm	7
BS	(33, 14, 23)	(33, 16, 21)	(33, 15, 22)	2.12 mm	3
BRW	(34, 24, 8)	(33, 21, 6)	(33, 24, 7)	2.12 mm	5
BA	(34, 34, 38)	(33, 34, 31)	(33, 34, 37)	2.12 mm	5
BLW	(35, 13, 46)	(33, 13, 43)	(38, 13, 44)	5.41 mm	4
BA	(36, 32, 35)	(33, 34, 31)	(33, 34, 35)	5.41 mm	4
BS	(37, 21, 19)	(40, 17, 21)	(35, 22, 18)	3.67 mm	15
BRW	(38, 18, 6)	(40, 22, 7)	(40, 21, 7)	5.61 mm	3
BP	(38, 8, 28)	(40, 6, 34)	(35, 7, 27)	4.97 mm	12
MA	(40, 30, 34)	(40, 34, 31)	(38, 33, 36)	6.18 mm	12
MP	(41, 5, 32)	(40, 6, 34)	(41, 5, 34)	3.00 mm	3
MLW	(41, 25, 45)	(40, 26, 41)	(41, 26, 43)	3.35 mm	3
MP	(43, 13, 8)	(40, 10, 9)	(42, 13, 9)	2.12 mm	6
MS	(45, 20, 18)	(40, 17, 21)	(45, 18, 20)	4.24 mm	7
AA	(50, 29, 28)	(47, 33, 31)	(49, 32, 28)	3.35 mm	6
AP	(50, 8, 25)	(47, 9, 20)	(52, 9, 25)	3.35 mm	5
AS	(55, 19, 25)	(54, 19, 24)	(54, 19, 24)	2.12 mm	4
ALW	(59, 16, 42)	(47, 17, 21)	(57, 16, 42)	5.15 mm	4
AA	(60, 23, 32)	(61, 28, 32)	(61, 25, 32)	3.35 mm	4

TABLE IV

SIMULATION RESULTS OF LOCALIZATION OF THE SITE OF ORIGIN OF VENTRICULAR ACTIVATION IN THE CASE OF CHANGED TORSO MODEL AND HEART POSITION

Ventricular Region		BA	BRW	BLW	BS	BP
True pacing site	(<i>i, j, k</i>)	(30, 33, 31)	(34, 24, 8)	(35, 13, 46)	(37, 21, 19)	(38, 8, 28)
Standard Model Inverse Solution	<i>DP</i> (<i>i, j, k</i>) <i>SD (mm)</i>	0 (33, 31, 31) 5.41	0 (33, 24, 7) 2.12	0 (38, 13, 44) 5.41	0 (35, 22, 18) 3.67	0 (35, 7, 27) 4.97
NTM+10% Inverse Solution	<i>DP</i> (<i>i, j, k</i>) <i>SD (mm)</i>	0 (33, 31, 31) 5.41	0 (32, 24, 7) 3.35	1 (38, 13, 44) 5.41	0 (38, 20, 21) 3.67	0 (37, 7, 31) 4.97
NTM-10% Inverse Solution	<i>DP</i> (<i>i, j, k</i>) <i>SD (mm)</i>	0 (33, 31, 31) 5.41	0 (33, 25, 7) 2.12	0 (38, 13, 44) 5.41	1 (35, 20, 18) 3.67	0 (37, 7, 31) 4.97
LSX Inverse Solution	<i>DP</i> (<i>i, j, k</i>) <i>SD (mm)</i>	0 (33, 31, 31) 5.41	0 (35, 25, 7) 2.60	0 (38, 14, 44) 5.61	0 (35, 22, 17) 4.50	0 (35, 6, 29) 5.61
RSX Inverse Solution	<i>DP</i> (<i>i, j, k</i>) <i>SD (mm)</i>	0 (33, 31, 31) 5.41	0 (33, 22, 8) 3.35	0 (38, 14, 44) 5.61	1 (35, 19, 18) 4.50	1 (35, 6, 29) 5.61
FSY Inverse Solution	<i>DP</i> (<i>i, j, k</i>) <i>SD (mm)</i>	0 (33, 31, 31) 5.41	0 (34, 24, 6) 3.00	0 (33, 13, 49) 5.41	0 (39, 20, 20) 3.67	0 (37, 7, 31) 4.97
BSY Inverse Solution	<i>DP</i> (<i>i, j, k</i>) <i>SD (mm)</i>	0 (33, 31, 31) 5.41	0 (33, 23, 7) 2.60	0 (33, 13, 49) 5.41	0 (38, 19, 20) 3.67	0 (37, 7, 31) 4.97

Table IV shows that the results of the PDS and inverse solutions for all five pacing sites in all six modified heart-torso models. In Table IV, the locations of the myocardial section of the true pacing site are shown under the ‘‘True pacing site.’’ The outcome of the PDS, the inversely localized site of the ec-

topic activation, as well as the spatial distance (SD) between the inverse site and the true site, are shown for each modified heart-torso model. For the sake of comparison, the inverse results when the standard heart-torso model was used are shown in the row of ‘‘Standard Model Inverse Solution.’’ In order to

show the deviation of the PDS due to the geometry errors, a deviation parameter (DP) was introduced as follows: DP = 0, when two myocardial segments are identical; DP = 1, when two myocardial segments are neighboring; DP = 2, when the two myocardial segments are separated by one myocardial segment; . . . In Table IV, the DP values refer to the distance between the initial myocardial segment identified by the PDS in a modified heart-torso model and that in the standard heart-torso model. Therefore, the DP values shown in Table IV reflect the effect of the geometry errors on the performance of the PDS.

From Table IV, it is noteworthy that while there is certain effect of the geometry errors on the initial estimate of the PDS, little effect of the heart-torso geometry uncertainty was observed on the final localization of site of ectopic activation using the present approach. This may be because the optimization system proposed in the present study is not sensitive to the initial guess when searching for the optimal solution.

IV. DISCUSSION

We have developed a new approach to localize the site of origin of cardiac activation in the 3-D myocardium, by incorporating *a priori* information regarding cardiac excitation and torso volume conduction. We use a parameter optimization system based on a 3-D computer heart model, instead of solving the matrix equation for the ECG inverse problem, to indirectly obtain the ECG inverse solution. The present heart-model-based electrocardiographic imaging approach is based on the unique and well-posed features of the ECG forward solution, the 3-D computer heart model in which *a priori* information regarding cardiac electrophysiology is incorporated, and the multiple objective functions, that contain the sensitive characteristics extracted from the BSPMs. The PDS based on an efficient ANN algorithm limits the searching space of heart model parameters, and effectively facilitates the convergence of the optimization system. The present approach not only circumvents two intrinsic difficulties of the ECG inverse problem, the nonuniqueness and ill-posedness, but also offer the desired solutions in terms of heart model parameters, that directly correspond to the cardiac physiological and pathological status (for example, the site of origin of cardiac activation or the site of origin of cardiac arrhythmias).

The PDS is a knowledge-based expert system. Development of the traditional expert systems based on knowledge-rules has met many challenges, for example, the “bottle-neck” problem in the knowledge-acquisition and the fragility. In the present study, we have successfully applied a three-layer feed-forward ANN to realize this expert system. The success rate of over 90% of the PDS (Table II) demonstrates the effectiveness of the ANN-based PDS. Tables II and III also indicate that the outcome of the PDS essentially affects only the number of iterations in the optimization procedure, but not the final result of pacing site localization.

In the present study, three characteristics of the BSPMs—the correlation coefficient (CC) between measured and simulated BSPMs, the location of the minimum in the measured and simulated BSPMs, and the area of negativity being less than

a certain negative threshold in the measured and simulated BSPMs—have been selected to construct the objective functions for the parameter optimization system. The characteristics, being used to construct an objective function of the optimization system, should be sensitive to the different pacing site while insensitive to intersubject variation. Fig. 4 suggests that the morphology of the BSPM is sensitive to the site of pacing. Based on observation of clinically measured BSPMs of an ectopic site, Benson *et al.* [23] reported that, when ventricular activation is primarily induced by an ectopic site, the pattern of BSPMs during QRS are reproducibly similar from patient to patient for a given site. Spach *et al.* [28] also reported that two major features govern the projection of epicardial events to the body surface: the magnitude of the epicardial potential gradients and the distance over which they exist on the epicardial surface (cardiac sources), and the distance to the recording area on the body surface (volume conductor). These experimental and clinical observations suggest that characteristics based on normalized parameters (e.g., regarding the heart-torso size) should be used in the parameter optimization procedure, and that intersubject variation may not have significant effect when the morphological pattern of the BSPM is concerned.

The effects of the geometry errors due to intersubject variation on the inverse solution have been addressed in a simulation for five pacing sites adjacent to the AV-ring. Modified heart-torso models simulating the torso geometry uncertainty and heart position uncertainty have been used in the forward calculation of the BSPMs due to pacing at each of the five representative locations. While some effects of these torso geometry and heart position uncertainties, as considered in the present study, are observed on the initial estimate of the myocardial segment of the PDS, little effects have been observed on the final localization of the site of origin of activation by the optimization system. These robust characteristics against geometry uncertainty may be due to the fact that the activation sequence instead of merely location of the source is taken into account in the present approach. The present simulation results are encouraging and promising, suggesting potential clinical applications of the present approach in localizing the site of origin of cardiac activation. However, while beyond the scope of the present manuscript, the effects of intersubject geometry variation should be further systematically addressed in the future investigations.

In the present simulation study, a pacing protocol has been used to simulate localized myocardial activation at different myocardial regions. Such protocol has been used previously in an experimental setting [29] and simulation setting [30]. To test the performance of the present approach to localize the site of origin of ventricular activation, twenty-four pacing sites from base to apex have been randomly chosen and performance examined. The present simulation results demonstrate the feasibility of localizing the site of origin of ventricular activation, with averaged localization errors for the 24 testing sites of being approximately equal to 3 ± 1.5 mm for $5\text{-}\mu\text{V}$ GWN and 4 ± 1.5 mm for $10\text{-}\mu\text{V}$ GWN. The present simulation study suggests that this new approach can provide a robust and accurate solution in localizing the site of origin of ventricular activation, may be applicable to clinical diagnosis of other cardiac diseases, and may become an important alternative to other ECG inverse solutions.

ACKNOWLEDGMENT

The authors would like to thank Prof. W. Lu and Dr. L. Xia of the Institute of Biomedical Engineering at Zhejiang University for valuable discussions.

REFERENCES

- [1] D. M. Mirvis, F. W. Keller, R. E. Ideker, J. W. Cox, R. J. Dowdie, and D. G. Zettergren, "Detection and localization of multiple epicardial electrical generators by a two-dipole ranging technique," *Circ. Res.*, vol. 41, pp. 551–557, 1977.
- [2] P. Savard, F. A. Roberge, J. Perry, and R. A. Nadeau, "Representation of cardiac electrical activity by a moving dipole for normal and ectopic beats in the intact dog," *Circ. Res.*, vol. 46, pp. 415–425, 1980.
- [3] R. M. Gulrajani, F. A. Roberge, and P. Savard, "Moving dipole inverse ECG and EEG solutions," *IEEE Trans. Biomed. Eng.*, vol. BME-31, pp. 903–910, 1984.
- [4] J. De Guise, R. M. Gulrajani, P. Savard, R. Guardo, and F. A. Roberge, "Inverse recovery of two moving dipoles from simulated surface potential distributions on a realistic human torso model," *IEEE Trans. Biomed. Eng.*, vol. BME-32, pp. 126–135, 1985.
- [5] D. B. Geselowitz, "Multipole representation for an equivalent cardiac generator," *Proc. IRE*, vol. 48, pp. 75–79, 1960.
- [6] J. J. M. Cuppen and A. van Oosterom, "Model studies with inversely calculated isochrones of ventricular depolarization," *IEEE Trans. Biomed. Eng.*, vol. BME-31, pp. 652–659, 1984.
- [7] G. Huiskamp and F. Greensite, "A new method for myocardial activation imaging," *IEEE Trans. Biomed. Eng.*, vol. 44, pp. 433–446, June 1997.
- [8] R. C. Barr, M. Ramsey III, and M. S. Spach, "Relating epicardial to body surface potential distributions by means of transfer coefficients based on geometry measurements," *IEEE Trans. Biomed. Eng.*, vol. BME-24, pp. 1–11, 1977.
- [9] R. C. Barr and M. S. Spach, "Inverse calculation of QRS-T epicardial potentials from normal and ectopic beats in the dog," *Circ. Res.*, vol. 42, pp. 661–675, 1978.
- [10] P. C. Frazone, B. Taccardi, and C. Viganotti, "An approach to the inverse calculation of epicardial potentials from body surface maps," *Adv. Cardiol.*, vol. 21, pp. 50–54, 1978.
- [11] A. V. Shahidi, P. Savard, and R. Nadeau, "Forward and inverse problems of electrocardiography: Modeling and recovery of epicardial potentials in humans," *IEEE Trans. Biomed. Eng.*, vol. 41, pp. 249–256, Mar. 1994.
- [12] R. D. Throne and L. G. Olson, "Generalized eigensystem techniques for the inverse problem of electrocardiography applied to a realistic heart-torso geometry," *IEEE Trans. Biomed. Eng.*, vol. 44, pp. 447–454, 1997.
- [13] P. R. Johnston and R. M. Gulrajani, "A new method for regularization parameter determination in the inverse problem of electrocardiography," *IEEE Trans. Biomed. Eng.*, vol. 44, pp. 19–39, Jan. 1997.
- [14] H. S. Oster, B. Taccardi, R. L. Lux, P. R. Ershler, and Y. Rudy, "Noninvasive electrocardiographic imaging: Reconstruction of epicardial potentials, electrograms, and isochrones and localization of single and multiple electrocardiac events," *Circulation*, vol. 96, pp. 1012–1024, 1997.
- [15] B. He, "On the Laplacian inverse electrocardiography," in *Proc. Ann. Int. Conf. IEEE Engineering in Medicine & Biology Society*, 1994, pp. 145–146.
- [16] B. He and D. Wu, "A bioelectric inverse imaging technique based on surface Laplacians," *IEEE Trans. Biomed. Eng.*, vol. 44, pp. 529–538, July 1997.
- [17] P. R. Johnston, "The Laplacian inverse problem of electrocardiography: An eccentric spheres study," *IEEE Trans. Biomed. Eng.*, vol. 44, pp. 539–548, July 1997.
- [18] B. He and R. J. Cohen, "Body surface Laplacian ECG mapping," *IEEE Trans. Biomed. Eng.*, vol. 39, pp. 1179–1191, Nov. 1992.
- [19] D. Wu, H. C. Tsai, and B. He, "On the estimation of the Laplacian electrocardiogram during ventricular activation," *Ann. Biomed. Eng.*, vol. 27, pp. 731–745, 1999.
- [20] L. Weixue, X. Zhengyao, and F. Yingjie, "Microcomputer-based cardiac field simulation model," *Med. Biol. Eng. Comput.*, vol. 31, pp. 384–387, 1993.
- [21] M. Aoki, Y. Okamoto, T. Musha, and K. Harumi, "Three-dimensional simulation of the ventricular depolarization and repolarization processes and body surface potentials: Normal heart and bundle branch block," *IEEE Trans. Biomed. Eng.*, vol. BME-34, pp. 454–462, 1987.
- [22] G. Li and W. Lu, "Improved neural network optimization algorithm for classification of imbalanced-exemplar patterns," *ACTA Elettronica SIN.*, vol. 16, pp. 123–125, 1998.
- [23] D. W. Benson, R. Sterba, J. J. Gallagher, A. Walston II, and M. S. Spach, "Localization of the site of ventricular preexcitation with body surface maps in patients with Wolff–Parkinson–White syndrome," *Circulation*, vol. 65, pp. 1259–1268, 1982.
- [24] M. Dubuc, R. Nadeau, G. Tremblay, T. Kus, F. Molin, and P. Savard, "Pace mapping using body surface potential maps to guide catheter ablation of accessory pathways in patients with Wolff–Parkinson–White syndrome," *Circulation*, vol. 87, pp. 135–143, 1993.
- [25] J. Kowalik and M. R. Osborne, *Methods for Unconstrained Optimization Problems*. New York: Elsevier, 1968.
- [26] R. Hren, B. B. Punske, and G. Stroink, "Assessment of spatial resolution of pace mapping when using body surface potentials," *Med. Biol. Eng. Comput.*, vol. 37, pp. 477–481, 1999.
- [27] R. H. S. Selvester, "Recommendation for nomenclature of myocardial subdivisions," *J. Electrocardiol.*, vol. 25, pp. 161–162, 1992.
- [28] M. S. Spach, R. C. Barr, C. F. Lanning, and P. C. Tucek, "Origin of body surface QRS and T wave potentials from epicardial distribution in the intact chimpanzee," *Circulation*, vol. 52, pp. 1030–1038, 1975.
- [29] A. Sippensgroenewegen, H. Spekhorst, N. M. Van Hemel, J. H. Kingma, R. N. W. Hauer, J. M. T. De Bakker, C. A. Grimbergen, M. J. Janse, and A. J. Dunning, "Localization of the site of the origin of postinfarction ventricular tachycardia by endocardial pace mapping: Body surface mapping compared with the 12-lead electrocardiogram," *Circulation*, vol. 88, pp. 2290–2306, 1993.
- [30] D. Wu, K. Ono, H. Hosaka, and B. He, "Simulation study of body surface Laplacian maps during induced ventricular activation: A model study," *Meth. Inform. Med.*, vol. 39, pp. 196–199, 2000.



Guanglin Li received the B.S. and M.S. degrees in electrical engineering from Shandong University of Technology, Jinan, China, in 1983 and 1988, respectively, and the Ph.D. degree in biomedical engineering from Zhejiang University, Hangzhou, China, in 1997.

In 1988, he joined the faculty of Electrical Engineering Department, Shandong University of Technology, and has been an Associate Professor since 1998. Since 1999, to present, he has been a Research Fellow in the Biomedical Functional Imaging and Computation Laboratory at the University of Illinois at Chicago. His research interests include electrocardiography forward and inverse problems, modeling and simulation of electrophysiological system, biomedical signal processing, and biomedical instrumentation.



Bin He (M'88–SM'97) received the Ph.D. degree in bioelectrical engineering with the highest honors from the Tokyo Institute of Technology, Tokyo, Japan, and completed the postdoctoral fellowship in biomedical engineering at Harvard University - MIT, Cambridge, MA.

After working at MIT as a Research Scientist, he joined the faculty of the University of Illinois at Chicago in 1994 and is currently an Associate Professor in bioengineering and electrical engineering, and the Director of the Biomedical Functional Imaging and Computation Laboratory. His major research interests include functional biomedical imaging, neural engineering, cardiovascular engineering, and computational biomedicine.

Dr. He is the recipient of the NSF CAREER Award, American Heart Association Established Investigator Award, and the University of Illinois University Scholar Award. He is listed in *Who's Who in Science and Engineering*, *Who's Who in America*, and *Who's Who in the World*. He has been active in professional activities, including editorial activities as the Guest Editor for *IEEE Engineering in Medicine and Biology Magazine*, *IEEE TRANSACTIONS ON INFORMATION TECHNOLOGY IN BIOMEDICINE*, *Critical Reviews in BME*, *Methods of Information in Medicine*, *Electromagnetics*, an Associate Editor for *IEEE TRANSACTIONS ON INFORMATION TECHNOLOGY IN BIOMEDICINE*. He serves as Vice President of the International Society of Bioelectromagnetism.